Internal Dynamics and Microwave Properties of *X*-Band Transferred-Electron Devices

RICHARD A. KIEHL, MEMBER, IEEE, AND ROBERT L. GUNSHOR, SENIOR MEMBER, IEEE

Abstract—**A study of the internal dynamics and microwave properties of an *X*-band transferred-electron device having ohmic contacts is reported. Numerical calculations of the electric field evolution and large-signal properties of the device have been carried out for frequencies throughout the 6–12-GHz range and for a wide range in ac voltage amplitude including amplitudes insufficient for space-charge quenching. An investigation is made of the influence of electron diffusion upon the field evolution and properties of the device. The large-signal admittance plane is determined and used to examine the behavior of the device in microwave circuits. A comparison is made between the calculated device properties and those of experimental devices.**

Circuit-controlled oscillation is found to be possible throughout the 6–12-GHz range for ac voltage amplitudes well below those required for space-charge quenching. At these amplitudes diffusion is shown to have a strong effect upon the electric field evolution and large-signal properties, and this effect is shown to bear significantly upon the behavior of the device in microwave circuits. Finally, the numerically calculated large-signal properties are found to agree reasonably well with experimental results.

I. Introduction

IN AN EFFORT to understand the behavior of transferred-electron devices undergoing interaction with microwave circuits, studies have been made of the effects that microwave terminal voltages have upon the internal dynamics of the device. In the earlier of these studies, where devices with long (approximately 100-μm) active regions were considered, it was shown that circuit-controlled oscillation is possible provided that the device–circuit interaction is such that the ac voltage amplitude is sufficiently large to delay or quench the growth of internal space-charge [1]–[3].

Models based upon this condition (which is commonly referred to as quenched- or delayed-mode operation) have been employed to characterize the device in terms of a large-signal admittance which can be used to determine the expected behavior of the device when interacting with a microwave circuit of known admittance [4]. While such models have provided results that are, to some extent, consistent with observed behavior, they do not account for the observed behavior of short (typically 10-μm) *X*-band devices at small ac voltage amplitudes. Experimental results indicate, for example, that such devices may undergo circuit-controlled oscillation even for ac voltage amplitudes insufficient for space-charge quenching [5], [6]. This device behavior, along with the behavior of the device as a stabilized amplifier at small voltage amplitudes [7] indicates that contrary to results for long devices, space-charge control is possible in short devices even for ac voltage amplitudes well below that required for space-charge delaying or quenching.

Space-charge control at small voltage amplitudes was recently demonstrated in computer simulations by Freeman and Hobson [8]. Their survey of *X*-band devices, which emphasized the important role played by cathode boundary conditions, indicated that the maximum device efficiency may, in fact, occur at such amplitudes. At present, however, little is known concerning the details of the internal dynamics and microwave properties of devices at these small amplitudes. In the present paper, we consider in detail the particular case of a device having ohmic contacts and investigate by numerical calculation the role that diffusion plays in determining the space-charge dynamics and microwave properties of such a device. We then characterize the microwave properties in terms of a large-signal admittance plane which is used to determine the expected behavior of the device in microwave circuits. Finally, we compare the calculated device properties with those of experimental devices.

In Sections II and III numerical calculations of the electric field evolution of the device for sinusoidal voltage waveforms with frequencies throughout the 6–12-GHz range are described. A wide range in ac voltage amplitude, including amplitudes insufficient for space-charge quenching, is considered for several different cases of the electron diffusion coefficient. In Section IV calculated current–voltage trajectories are used to relate the internal dynamics to the microwave properties of the device which are then characterized in terms of large-signal admittance planes. In Section V the large-signal admittance planes are used to examine the behavior of the device in microwave circuits, and a comparison is made between the calculated admittance and the admittance of experimental devices. Finally, conclusions are given in Section VI.

II. Device Model

The internal dynamics of the device are taken to be described by the equation of total current I as given by

$$\frac{I(t)}{A} = qn(x,t)v(E) - qD(E)\frac{\partial n}{\partial x} + \varepsilon\frac{\partial E}{\partial t} \tag{1}$$

and Poisson's equation

$$\frac{\partial E}{\partial x} = \frac{q}{\varepsilon}[n(x,t) - n_0(x)] \tag{2}$$

Manuscript received April 16, 1975; revised November 12, 1975. This work was supported in part by the National Science Foundation under Grant GK-11958, and in part by the Purdue NSF/MRL Program.

R. A. Kiehl was with the School of Electrical Engineering, Purdue University, West Lafayette, IN 47906. He is now with Sandia Laboratories, Albuquerque, NM 87111.

R. L. Gunshor is with the School of Electrical Engineering, Purdue University, West Lafayette, IN 47906.

where E is the electric field intensity at position x for time t, where q, ε, n_0, v, and D are the electronic charge, dielectric constant, doping density, electron drift velocity, and electron diffusion coefficient, respectively, and where the usual assumptions that current is uniform over the cross-sectional area A and carried only by electrons of density n have been made.

Using (2) to eliminate the electron density from (1), we write the equation of total current in terms of E giving

$$\frac{I(t)}{A} = \varepsilon v(E)\frac{\partial E}{\partial x} + qv(E)n_0(x) - \varepsilon D(E)\frac{\partial^2 E}{\partial x^2} - qD(E)\frac{\partial n_0}{\partial x} + \varepsilon\frac{\partial E}{\partial t}. \quad (3)$$

Ohmic contacts are assumed and hence we take

$$E(0,t) = E(l,t) = 0 \quad (4)$$

where l is the length of the active region. In order to simulate the waveform constraints of a high-Q, parallel resonant circuit, the external circuit is taken to consist of an ac and a dc voltage source and a low-valued series resistance. That is, we require that

$$I(t) = \frac{V_B + V_0 \sin(2\pi f_0 t) - V(t)}{R} \quad (5)$$

where the device voltage V is given by

$$V(t) = \int_0^l E(x,t)\,dx. \quad (6)$$

The value of R in (5) is chosen to be sufficiently small to ensure that the device voltage waveform is essentially sinusoidal and the values of V_B, f_0, and V_0 are chosen to determine the dc component V_{dc}, frequency f, and ac component V_{ac} of this waveform.

The numerical solution to (3), (5), and (6), together with the boundary conditions of (4) and the initial conditions $I(0) = 0$, $V(0) = V_B$, and $E(x, 0) = V_B/l$, is obtained by a finite-difference technique [10]. This solution is calculated over several quasi-cycles until a steady state is reached.

Throughout this study the field dependence of the electron drift velocity is taken to be that given by Ruch and Fawcett [11] for a uniform lattice temperature of 450 K and the doping profile is assumed to be flat. The values of the doping density, active-region length and area, which were chosen to approximate those of the experimental devices described in Section V, are 1.9×10^{15} cm^{-3}, 10 μm, and 1.66×10^{-4} cm^2, respectively. The dielectric constant equals 1.106×10^{-12} F/cm and, unless specified otherwise, R equals 2 Ω.

Several different electron diffusion coefficients are used in the calculations. Although the diffusion coefficient in GaAs is known to depend upon the electric field, the various experimental and theoretical estimates of this dependence differ considerably for fields slightly above threshold [9]. Since the gradient of electron density is highest for these fields, it is at such fields that the space-charge dynamics are most sensitive to the level of diffusion [12]. Hence, the diffusion coefficients in this study have been chosen to represent low, moderate, and high postthreshold diffusion levels in accordance with the various experimental and theoretical estimates. Specifically, for low and moderate diffusion, D is taken to be constant and equal to 200 cm^2/s and 300 cm^2/s, respectively. For high diffusion, D is taken to be the Copeland characteristic [13]. The diffusion level of this characteristic is approximately 500 cm^2/s at fields slightly above threshold and decreases to 200 cm^2/s for low fields. Such a field-dependent characteristic was chosen for the high-diffusion case since using a constant value for this case would have resulted in a low-field diffusion level that is too high, according to all of the experimental and theoretical estimates.

The preceding mathematical description is based upon the familiar, simplified two-valley model [3], [14] in which the distribution of electrons among the two valleys is taken to depend locally and instantaneously on the electric field, and carrier transport is described in terms of the density and average velocity of the electrons considered as a single gas. Hence no attempt is made here to consider energy relaxation and thermoelectric effects which can be properly treated only by more complex models [15, [16].

III. Electric Field Evolution

In this section we describe the results of an investigation of the influences that the amplitude and frequency of the ac voltage across the device as well as the electron diffusion processes within the device have upon the electric field evolution. The field evolution and current waveform were obtained by numerically calculating the response of the device to essentially sinusoidal voltage waveforms having frequencies f throughout the 6–12-GHz range and amplitudes V_{ac} throughout a range from 9 V to less than 1 V. The dc component of the device voltage was always 10 V. A typical calculated device voltage waveform $V(t)$ is shown in Fig. 1. In this and subsequent figures the time axis is normalized to one ac period and numbering refers to equally spaced time instants.

For the two higher diffusion cases the ac voltage was found to control the field evolution, providing periodic waveforms after just a few cycles, throughout the entire amplitude and frequency ranges. This was found to be true despite the fact that amplitudes less than about 6.5 V were insufficient for space-charge quenching. For the lowest diffusion case such control was possible for amplitudes greater than 1 or 2 V; however, for smaller amplitudes, periodic waveforms sometimes did not occur even after

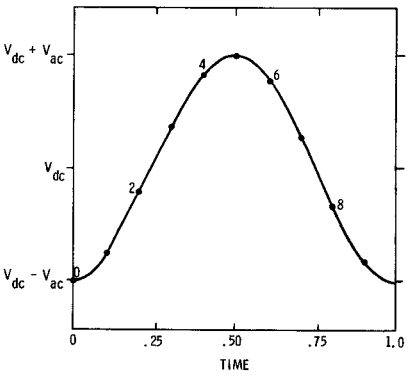

Fig. 1. Device voltage waveform.

many simulated "cycles." The inability to control space charge at such small voltage amplitudes for this diffusion case was found to be related to the instability of the device in the resistive biasing circuit. This point will be discussed further in Section V.

The influence that electron diffusion processes had upon the field evolution was found to depend upon both the amplitude of the voltage waveform and its frequency.

A. Amplitude Dependence

At amplitudes greater than about 6.5 V, for which space-charge quenching occurred, the electric field evolution was found, for all cases of diffusion, to be that of the usual traveling accumulation layer nucleated at the cathode by the rising electric field. This is shown in Fig. 2 for $V_{ac} = 7$ V and $D = 200$ cm^2/s. The field evolutions calculated for the two higher diffusion cases were almost identical, with differences being due simply to a slight broadening of the space-charge layers.

At amplitudes less than 6.5 V, however, electron diffusion was found to have a strong effect upon the field evolution, even to the point of influencing the type of space-charge mode that occurred. This is shown in Figs. 3–5 for $V_{ac} =$ 4.5 V. The importance of diffusion at amplitudes insufficient for space-charge quenching can be seen to be due to the effect that the diffusion of the space-charge remaining at the end of one ac cycle has upon the device dynamics during the voltage rise of the following cycle. Fig. 3 shows that for low diffusion the space-charge region cannot widen rapidly enough to support much of the voltage increase occurring between time instants 0 and 1; hence the low-field region rapidly rises above threshold, thus nucleating a traveling accumulation layer. Essentially, the same is true for Fig. 4, the only difference being that the somewhat higher diffusion considered in this figure causes the nucleation to occur later in time. In the high-diffusion case of Fig. 5, however, the space-charge region widens rapidly enough to support a large enough portion of the increasing terminal voltage such that the low-field region never exceeds threshold. In this

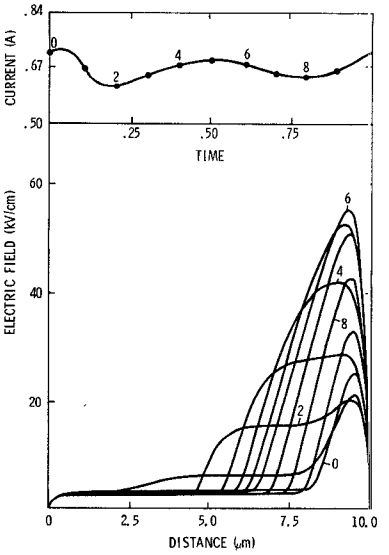

Fig. 3. Current waveform and electric field evolution for $D =$ 200 cm^2/s, $V_{ac} = 4.5$ V, and $f = 8$ GHz.

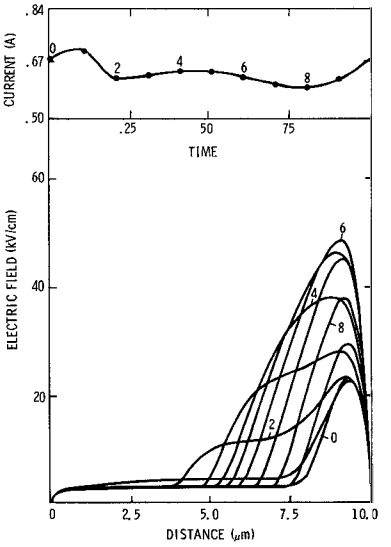

Fig. 4. Current waveform and electric field evolution for $D =$ 300 cm^2/s, $V_{ac} = 4.5$ V, and $f = 8$ GHz.

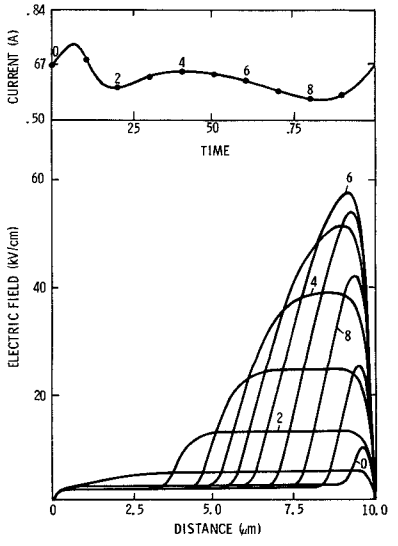

Fig. 2. Current waveform and electric field evolution for $D =$ 200 cm^2/s, $V_{ac} = 7.0$ V, and $f = 8$ GHz.

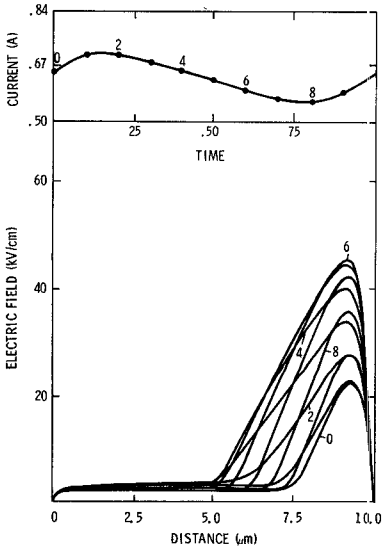

Fig. 5. Current waveform and electric field evolution for the Copeland diffusion coefficient, $V_{ac} = 4.5$ V, and $f = 8$ GHz.

case, therefore, no accumulation layer is nucleated, and instead the field evolution is more that of a modulated, anode-adjacent domain. Thus, in general, increasing diffusion was found to cause a gradual transition to occur in the space-charge mode from a traveling accumulation layer to a modulated anode-adjacent domain.

B. Frequency Dependence

The field evolutions shown in Figs. 2–5 were calculated for a voltage waveform having a frequency of 8 GHz. Calculations were also made at 6, 10, and 12 GHz. Differences in the field evolutions calculated at various frequencies were found to be due mainly to transit-time effects which caused a larger portion of the time-averaged electric field to be above threshold at higher frequencies. At sufficiently low frequencies, however, in addition to transit-time effects, diffusion processes were found to be important. At frequencies below about 8 GHz, the period is sufficiently long that the accumulation layer transits almost the entire length of the active region, forming an anode-adjacent domain, before the voltage has ceased to rise. The dynamics of this domain during the remainder of the voltage rise were found to be strongly influenced by diffusion. For low diffusion, it was found that the space-charge layer did not widen rapidly enough to support much of the increase in voltage and thus the low field rose above threshold nucleating a second traveling accumulation layer. This is shown in Fig. 6 which was calculated for a frequency of 6 GHz. For higher diffusion coefficients, for which the space-charge region widens more rapidly, no second layer was found to form. The results show that, depending on the level of diffusion, the dynamics of the device may change rather abruptly with frequency.

IV. Microwave Properties

In the previous section numerical calculations were used to investigate the internal dynamics of the device. In this section we relate the internal dynamics to the microwave properties of the device and characterize these properties in terms of large-signal admittance planes.

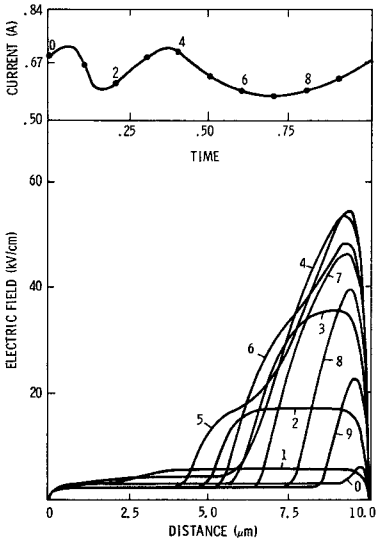

Fig. 6. Current waveform and electric field evolution for the same case as shown in Fig. 2, but $f = 6$ GHz.

A. Current–Voltage Relationships

Differences in the electric field evolutions for the various diffusion cases shown in Figs. 3–5 result in differences in the current waveforms and hence the microwave properties of the device. The influence of diffusion upon the microwave properties may be illuminated by examining the current–voltage phase relationships of the device dynamics.

First consider the second half-cycle in these figures, i.e., time instants 6 through 0. For this half-cycle the field evolution for all of the diffusion cases represents the discharging of an anode-adjacent domain. This discharge mechanism is capacitive in nature. Hence the phase relationship between the voltage and current waveforms during the second half-cycle is capacitive for all of the diffusion cases, as can be seen from the figures. Now consider the first half-cycle, i.e., time instants 1 through 5. For the high-diffusion case of Fig. 5, the field evolution for this half-cycle represents the charging of an anode-adjacent domain, and as in the second half-cycle, results in a capacitive phase relationship. The same is not true, however, for the lower diffusion cases. As shown in Fig. 3, the nucleation and propagation of a traveling accumulation layer for the low-diffusion case causes a current minimum, rather than a maximum, to occur near the middle of the first half-cycle. Hence, although the current–voltage phase relationship for this case is capacitive during the second half-cycle, during the first half-cycle it is inductive. Essentially, the same is true for the intermediate diffusion case of Fig. 4 except that the nucleation of the accumulation layer occurs later in time resulting in a somewhat less inductive waveform.

These phase relationships are clearly illustrated by the current–voltage trajectories shown in Fig. 7. It can be seen that for the high-diffusion case the direction of rotation is always clockwise indicating that a capacitive phase relationship occurs throughout the entire ac cycle. The nearly elliptical shape of the trajectory is attributable to the essentially linear nature of a modulated, anode-adjacent domain. For the lower diffusion cases, the direction of rotation is counterclockwise from approximately instants 1 through 5, indicating an inductive phase relationship over this portion of the cycle. At instant 5, however, the direction of rotation reverses and a capacitive phase relationship occurs over the

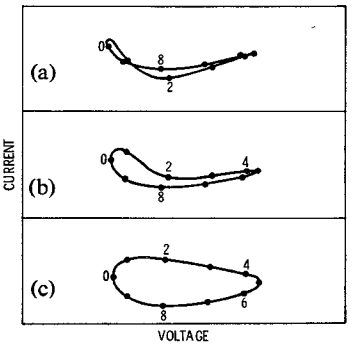

Fig. 7. Current–voltage trajectory for $V_{ac} = 4.5$ V. (a) $D = 200$ cm^2/s. (b) $D = 300$ cm^2/s. (c) The Copeland diffusion coefficient.

remainder of the cycle. The highly nonelliptical shapes of these trajectories are attributable to the highly nonlinear dynamics of accumulation-layer nucleation.

The foregoing discussion shows that a competition between capacitive and inductive space-charge dynamics results in microwave properties that tend to be more inductive and more nonlinear for lower diffusion coefficients.

B. Large-Signal Admittance

The microwave properties of the device may be characterized by a large-signal admittance $Y_D(f,V_{ac})$ which is a function of the amplitude as well as the frequency of the device voltage. This large-signal admittance was determined for each case of diffusion by Fourier analysis of a large number of numerically calculated voltage and current waveforms.

The results are given in Figs. 8–10 where lines of constant frequency, marked at 2-V intervals in amplitude, have been plotted. It can be seen from these figures that, consistent with the preceding discussion, decreased diffusion causes a significant increase in the ranges of conductance and susceptance exhibited by the device.

V. Device–Circuit Interactions

In this section we make use of the results of the large-signal admittance calculations to examine the behavior of the device when interacting with microwave circuits, and we compare the admittance calculations with results for experimental devices.

A. Purely Conductive Circuits

In recent studies of the stabilization mechanisms that occur in devices similar to those of this study, it has been shown that diffusion has a significant influence upon the stability of the device in a purely conductive circuit [9], [12]. Consistent with the results of these studies, in the present study it was found that when biased in high-conductance circuits with no external ac voltage applied [$V_0 = 0$ in (5)] the device stabilized with the formation of a stationary anode-adjacent domain for the two higher diffusion cases;

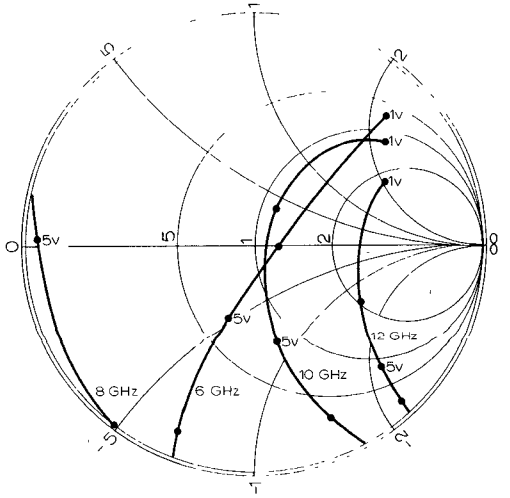

Fig. 8. Negative of the device admittance $Y_D(f, V_{ac})$ for D = 200 cm²/s. Values are normalized to 10^{-2} mho.

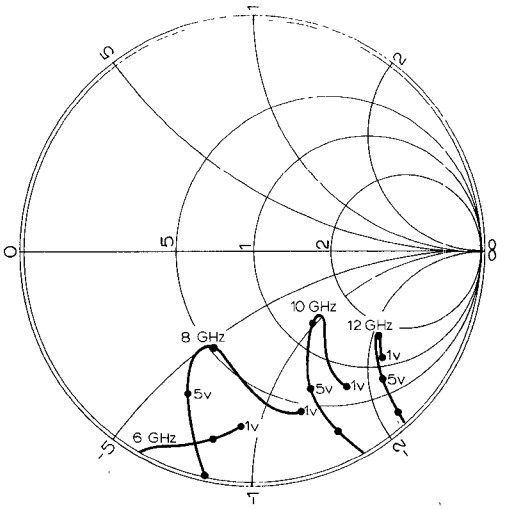

Fig. 9. Negative of the device admittance $Y_D(f, V_{ac})$ for D = 300 cm²/s. Values are normalized to 10^{-2} mho.

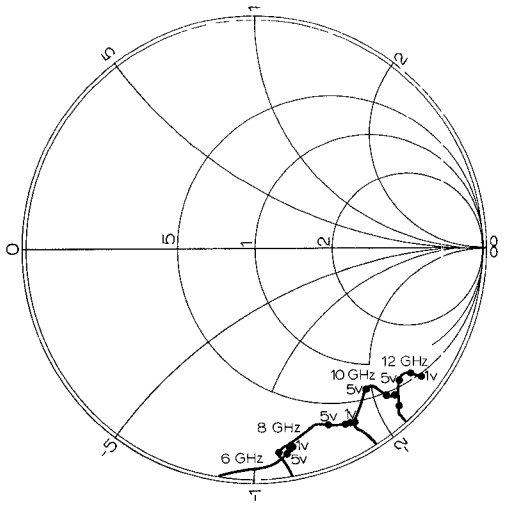

Fig. 10. Negative of the device admittance $Y_D(f, V_{ac})$ for the Copeland diffusion coefficient. Values are normalized to 10^{-2} mho.

while for the low-diffusion case, oscillation occurred due to the periodic injection of traveling accumulation layers. Specifically, oscillations of 1–2-V amplitude were found to occur at 10.1, 11.1, and 15.2 GHz in purely conductive circuits of 20, 30, and 500 mmho, respectively.

The influence of diffusion upon this device–circuit interaction can be understood in terms of the effect that diffusion has upon the device admittance Y_D. Since the device is capacitive at all voltage amplitudes for the two higher diffusion cases of Figs. 9 and 10, the condition

$$Y_C(f) + Y_D(f,V_{ac}) = 0 \qquad (7)$$

cannot be satisfied in purely conductive circuits of admittance Y_C and hence for these diffusion cases, free-running oscillations with sinusoidal voltage waveforms cannot be sustained [17] (assuming, of course, that (7) is not satisfied at frequencies outside the 6–12-GHz range). However, since the device susceptance is zero at some amplitudes for the low-diffusion case of Fig. 8, for this case, oscillation may be sustained at a frequency and amplitude governed by (7).

From the foregoing discussion and that of Section III, it can be seen that oscillatory behavior is possible in purely conductive circuits for sufficiently low diffusion coefficients due to the occurrence of a zero in device susceptance that comes about due to an internal tuning of the dielectric and anode-adjacent domain capacitance by the inductive effect of the accumulation-layer injection. We mention here that such oscillation is responsible for it not having been possible to control space-charge for the low-diffusion case when the amplitude was less than about 1 V, as noted in Section III.

B. Resonant Waveguide Circuits

Here we examine the device behavior in a typical microwave oscillator circuit consisting of an S4 package mounted at the bottom of a 0.307-cm-diam cylindrical post that is centered in an *X*-band waveguide. One arm of the waveguide is taken to contain a shorting plunger positioned at a variable distance L from the center of the post. This circuit has been described in detail elsewhere [18], [19]. We employ the analytical circuit model given by Jethwa and Gunshor [18] and the S4 package model given by Owens and Cawsey [20] to determine the admittance $Y_C(f)$ presented by the circuit to the device chip.

Figs. 11 and 12 show $Y_C(f)$ for two different values of L. Note that the general effect of decreasing L is to cause a counterclockwise rotation (increase in resonant frequency) and contraction of the $n\lambda_g/2$ guide-mode resonances. (Both the $\lambda_g/2$ and λ_g resonances occur below 12 GHz for L = 3 cm, while only the $\lambda_g/2$ occurs for L = 2 cm.) With reference to Figs. 8–10 it can be seen, therefore, that the device behavior for small L (high frequencies) will be strongly dependent upon its properties at small ac amplitudes where maximum negative conductance occurs and hence will depend strongly on diffusion. In particular, these figures indicate that diffusion bears significantly upon the tuning range of the device in such a circuit.

The microwave properties of the device at its oscillatory

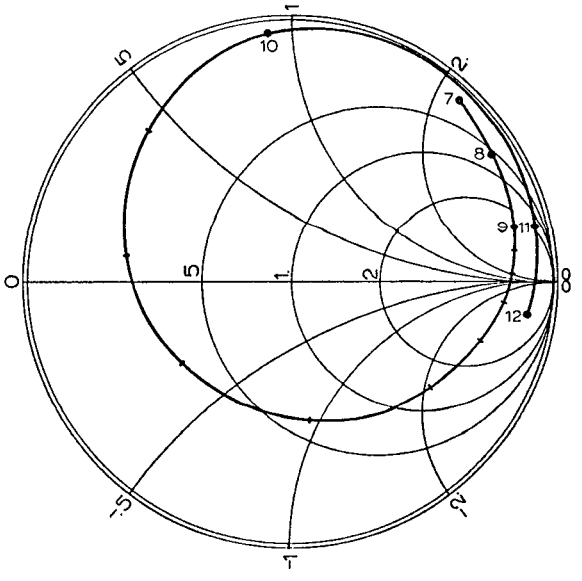

Fig. 11. Circuit admittance $Y_C(f)$ for the short position L equal to 2 cm.

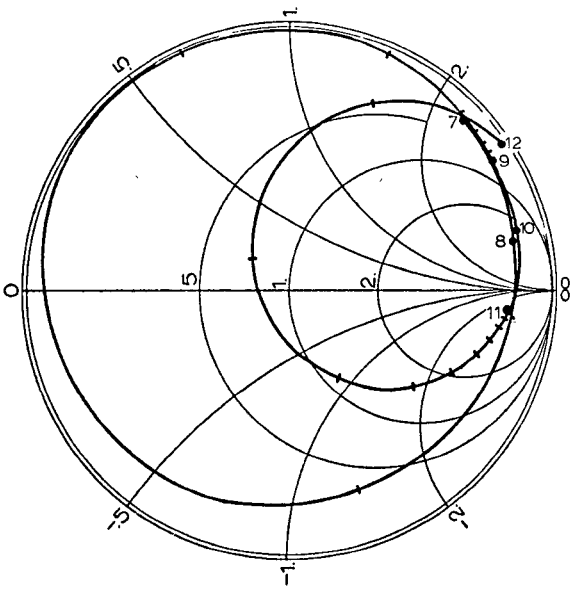

Fig. 12. Circuit admittance $Y_C(f)$ for the short position L equal to 3 cm.

operating point (f,V_{ac}) were determined as a function of L for the intermediate diffusion case by constructing the device admittance $Y_D(f,V_{ac})$ by interpolation from Fig. 9 and solving (7) numerically. In so doing, we were careful to ignore unstable operating points [17]. Only solutions corresponding to the $\lambda_g/2$ resonance were sought, although solutions corresponding to the λ_g resonance were also possible for large L. Figs. 13 and 14 show the resulting ac voltage amplitude and large-signal admittance of the device at its operating point. In agreement with the preceding qualitative discussion, the results show that for this intermediate diffusion case, oscillation is possible for a large range in L corresponding to frequency tuning from approximately 7.2–12.0 GHz (as L is decreased). It is important to note that for L less than about 2.5 cm the magnitude of the device conductance increases rapidly with decreasing L and that the ac voltage amplitude is small over a significant portion of the tuning range.

C. Experimental Devices in Resonant Waveguide Circuits

Experimental measurements were made on a number of actual devices undergoing oscillation in the resonant waveguide circuit previously described. The devices, which were obtained from Microwave Associates, were of n^+-n-n^+ construction and had specified values for active length, active area, and doping concentration that were the same as those used in the numerical calculations described in Section II. As was taken to be the case in the calculations, the experimental devices were biased at 10 V.

Oscillation at a frequency corresponding to the $\lambda_g/2$ resonance was found to occur for L between approximately 2 and 5 cm (f between approximately 9.5 and 7.5 GHz). Within this range, smooth tuning along the $\lambda_g/2$ resonance curve occurred for devices designated *A* and *B*. The device designated *C* tuned similarly over most of this range, but for some L exhibited a jump to a higher frequency corresponding either to the λ_g resonance or to the slab-line

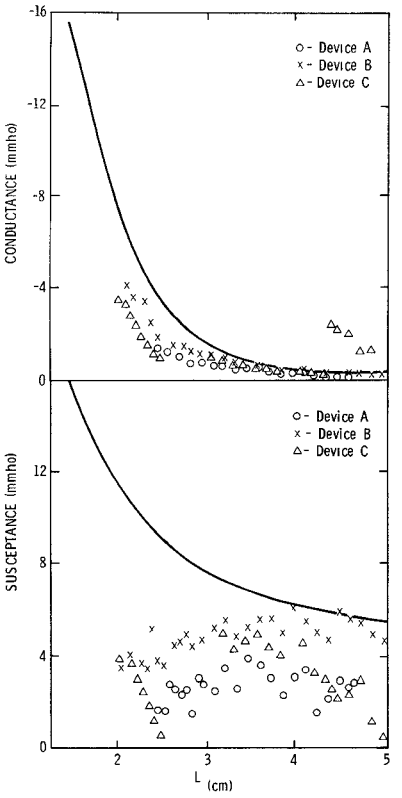

Fig. 13. Device conductance and susceptance as a function of short position. Solid curves give the theoretical values for the intermediate-diffusion case.

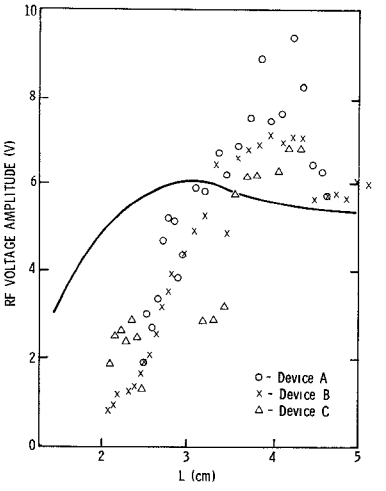

Fig. 14. Device ac voltage amplitude as a function of short position. Solid curve gives the theoretical values for the intermediate-diffusion case.

resonance [18], [19]. For L less than 2 cm the devices exhibited weak oscillation at the slab-line resonance or ceased oscillation altogether.

Measurements of the frequency and power of the $\lambda_g/2$ oscillations were made as a function of L and were used to determine the ac voltage amplitude and large-signal admittance of the device at its oscillation frequency as given by (7) and the relation

$$V_{ac} = \sqrt{\frac{2P}{|G_D|}} \tag{8}$$

where P is the measured power and G_D is the experimentally determined device conductance.

The results are shown in Figs. 13 and 14. It can be seen that for large L a reasonably good agreement exists between these results and the theoretical curves of the intermediate-diffusion case. For small L the results show that the amplitude was somewhat less for the experimental devices and that for these devices oscillation was not possible for as small an L. Recalling that the effect of decreasing L is to contract the circuit resonance circles, one can see that these differences indicate that the maximum negative conductance of the experimental devices is less than that calculated for the intermediate-diffusion case. It has already been seen in Figs. 8–10 that a larger diffusion coefficient results in a lower maximum device conductance. Hence the differences between theory and experiment in Figs. 13 and 14 can, to a large degree, be accounted for by an electron diffusion coefficient that is somewhat larger than that of the intermediate-diffusion case, but still less than that of the high-diffusion case. Although nonohmic contacts and other effects not included in the present device model might also contribute to such differences, it may be concluded that within the bounds for diffusion considered in this study the theoretical microwave properties of the device are in reasonable agreement with the properties of experimental devices.

VI. Conclusion

A numerical study of the internal dynamics and microwave properties of an X-band transferred-electron device having ohmic contacts has been described. It was demonstrated that, in contrast to results for long devices, a short X-band device may undergo circuit-controlled oscillation over a wide frequency range even for ac voltage amplitudes well below that required for space-charge quenching or delaying. The results emphasize, therefore, that device models based upon a quenching or delaying of space-charge by large ac voltage swings are inadequate for explaining the complete behavior of X-band devices.

The dependence of the device electric field evolution and large-signal admittance upon the level of electron diffusion was examined. It was shown that due to the importance of diffusion in the readjustment of space-charge remaining at the end of the ac cycle, diffusion processes strongly influence the field evolution and large-signal admittance of the device at small ac voltage amplitudes. This effect was shown to bear significantly upon the behavior of the device in microwave circuits.

Finally, calculations of the large-signal properties of the device were shown to agree reasonably well with experimental results for devices undergoing oscillation in a typical X-band oscillator circuit.

References

[1] J. A. Copeland, "Theoretical study of a Gunn diode in a resonant circuit," *IEEE Trans. Electron Devices*, vol. ED-14, pp. 55–58, Feb. 1967.
[2] T. Ikoma and H. Yanai, "Effect of external circuits on Gunn oscillation," *IEEE J. Solid-State Circuits*, vol. SC-2, pp. 108–113, Sept. 1967.
[3] P. R. Solomon, M. P. Shaw, and H. L. Grubin, "Analysis of bulk

negative differential mobility element in a circuit containing reactive elements," *J. Appl. Phys.*, vol. 43, pp. 159–172, Jan. 1972.
[4] D. D. Khandelwal and W. R. Curtice, "A study of the single-frequency quenched-domain mode Gunn-effect oscillator," *IEEE Trans. Microwave Theory Tech.*, vol. MTT-18, pp. 179–187, Apr. 1970.
[5] W. R. Curtice, "Quenched-domain mode oscillation in waveguide circuits," *IEEE Trans. Microwave Theory Tech.*, vol. MTT-21, pp. 369–374, June 1973.
[6] G. S. Hobson, "Some properties of Gunn-effect oscillations in a biconical cavity," *IEEE Trans. Electron Devices (Special Issue on Semiconductor Bulk-Effect and Transit-Time Devices)*, vol. ED-14, pp. 526–531, Sept. 1967.
[7] B. S. Perlman, "CW microwave amplification from circuit-stabilized epitaxial GaAs transferred-electron devices," *IEEE J. Solid-State Circuits (Special ISSCC Issue on Solid-State Microwave Circuits)*, vol. SC-5, pp. 331–337, Dec. 1970.
[8] K. R. Freeman and G. S. Hobson, "A survey of CW and pulsed Gunn oscillators by computer simulation," *IEEE Trans. Electron Devices*, vol. ED-20, pp. 891–903, Oct. 1973.
[9] P. Jeppesen and B. Jeppsson, "The influence of diffusion on the stability of supercritical transferred electron amplifiers," *Proc. IEEE* (Lett.), vol. 60, pp. 452–454, Apr. 1972.
[10] R. A. Kiehl, "The internal dynamics and microwave properties of *X*-band transferred-electron devices," Ph.D. dissertation, Purdue Univ., Lafayette, IN, 1974.
[11] J. G. Ruch and W. Fawcett, "Temperature dependence of the transport properties of gallium arsenide determined by a Monte Carlo method," *J. Appl. Phys.*, vol. 41, pp. 3845–3850, Aug. 1970.
[12] P. Jeppesen and B. I. Jeppsson, "A simple analysis of the stable field profile in the supercritical TEA," *IEEE Trans. Electron Devices*, vol. ED-20, pp. 371–379, Apr. 1973.
[13] J. A. Copeland and S. Knight, "Applications utilizing bulk negative resistance," in *Semiconductors and Semimetals*, vol. 7A, R. K. Williardson and A. C. Beer, Ed. New York: Academic, 1971, pp. 3–72.
[14] H. Kroemer, "Nonlinear space-charge domain dynamics in a semiconductor with negative differential mobility," *IEEE Trans. Electron Devices (Special Issue on Semiconductor Bulk-Effect and Transit-Time Devices)*, vol. ED-13, pp. 27–40, Jan. 1966.
[15] K. Blotekjaer, "Transport equations for electrons in two-valley semiconductors," *IEEE Trans. Electron Devices*, vol. ED-17, pp. 38–47, Jan. 1970.
[16] D. Jones and H. D. Rees, "Electron-relaxation effects in transferred-electron devices revealed by new simulation method," *Electron. Lett.*, vol. 8, pp. 363–364, July 1972.
[17] K. Kurokawa, "Some basic characteristics of broadband negative resistance oscillator circuits," *Bell Syst. Tech. J.*, vol. 48, pp. 1937–1955, July 1969.
[18] C. P. Jethwa and R. L. Gunshor, "An analytical equivalent circuit representation for waveguide-mounted Gunn oscillators," *IEEE Trans. Microwave Theory Tech.*, vol. MTT-20, pp. 565–572, Sept. 1972.
[19] R. L. Eisenhart and P. J. Khan, "Some tuning characteristics and oscillation conditions of waveguide-mounted transferred-electron diode oscillator," *IEEE Trans. Electron Devices*, vol. ED-19, pp. 1050–1055, Sept. 1972.
[20] R. P. Owens and D. Cawsey, "Microwave equivalent-circuit parameters of Gunn-effect-device packages," *IEEE Trans. Microwave Theory Tech., (Special Issue on Microwave Circuit Aspects of Avalanche-Diode and Transferred Electron Devices)*, vol. MTT-18, pp. 790–798, Nov. 1970.

Filters with Single Transmission Zeros at Real or Imaginary Frequencies

RALPH LEVY, FELLOW, IEEE

Abstract—**A new unified theory is presented for the synthesis of exactly equiripple low-pass prototypes having: a) one simple pole of attenuation at a real frequency; or b) a single pair of real-axis transmission zeros (giving linear-phase performance). These types of filters may be regarded as representing the least possible degree of complication over the conventional Chebyshev filter, and are usually realized with one extra cross coupling in the structure. It is demonstrated that this gives much improved skirt selectivity in the case of a finite frequency pole, making it a viable intermediate case between the Chebyshev and elliptic-function filters, while in the case of real-frequency zeros, very flat group delay over 50 percent of the passband is achieved with minimal cost in insertion loss and skirt rejection. Approximate and exact synthesis techniques are described, including results for the previously neglected odd-degree case. Experimental results demonstrate agreement with theory.**

I. Introduction

THIS PAPER describes two classes of filters which have quite distinct applications, yet are closely related mathematically and in physical realization. They are distinguished by the location of their transmission zeros (attenuation poles), which, in the case of the first class, are at real frequencies, and in the case of the second class are at imaginary frequencies (i.e., on the real axis of the complex frequency plane). In this paper filters having only one pair of transmission zeros are described, not only because these cases may be synthesized exactly with no difficulty, but also because they give important substantial improvements compared with conventional Chebyshev equiripple filters, yet with little practical difficulty of physical realization.

The transmission zeros may be realized by cross coupling a pair of nonadjacent elements of the filter, negatively to give real-frequency transmission zeros, positively to give real-axis zeros. The first type of filter gives improved skirt attenuation performance, and the second gives improved passband delay characteristics compared with the ordinary Chebyshev filter.

The first application of coupling between nonadjacent resonators at microwave frequencies appears to have originated with Kurzrok [1], [2]. He showed that to obtain finite frequency attenuation poles it was necessary to

Manuscript received July 18, 1975; revised October 27, 1975.
The author is with the Microwave Development Laboratories, Natick, MA 01760.